

# TiO<sub>2</sub> Branched Nanostructure Anode Material Prepared by Seeding Method for High-performance Lithium Ion Batteries

Biao Han<sup>1</sup>, Si-Jin Kim<sup>1</sup>, Bo-Mi Hwang<sup>1</sup>, Eui-Tak Hwang<sup>1</sup>, Han Chul Park<sup>1</sup>,  
Mun-Hyun Koh<sup>2</sup>, and Kyung-Won Park<sup>1,\*</sup>

<sup>1</sup>*Department of Chemical Engineering, Soongsil University, Seoul 156-743, Korea*

<sup>2</sup>*College of Law, Soongsil University, Seoul 156-743, Korea*

(Received March 14, 2013 : Accepted April 6, 2013)

**Abstract :** We demonstrate rutile TiO<sub>2</sub> branched nanostructure (TiO<sub>2</sub>-BN) electrodes synthesized by seeding method for enhanced lithium intercalation properties. The morphology and crystal-line nature of the TiO<sub>2</sub>-BN were clearly observed by field-emission transmission electron microscopy and fast Fourier transform pattern. The TiO<sub>2</sub>-BN electrodes showed excellent capacity and high rate performance. The improved lithium-ion intercalation properties of the TiO<sub>2</sub>-BN may be attributed to relatively large specific surface area and short transport distance of the branched nanostructure.

**Keywords :** Branched nanostructure, Lithium ion battery, Rutile, TiO<sub>2</sub>

## 1. Introduction

Lithium-ion batteries (LIBs) are essential portable power sources because of their high-energy density, high-power density, and long cycle life.<sup>1,2)</sup> Typically, graphite-based materials have been a typical anode material to apply commercial LIBs. Because of several disadvantages of graphite anode materials such as initial capacity loss and structural deformation, it is urgently required to develop novel materials and structures with high-performance lithium intercalation.<sup>3,4)</sup> As an alternative of graphite, titanium dioxide (TiO<sub>2</sub>) utilized in a variety of applications such as photocatalytic activity,<sup>5,6)</sup> catalyst supports,<sup>7)</sup> and gas sensors<sup>8)</sup> is regarded as a promising lithium insertion/extraction material with low production cost and high capacity.<sup>9)</sup>

TiO<sub>2</sub> nanostructured materials such as nanorods, nanowires, and nanotubes have been studied in order to achieve excellent LIBs with high energy density, large capacity, rate performance and long cycle life.<sup>10,11)</sup> Considerable efforts have been made to explore diverse synthetic methods ranging from

vapor-phase techniques to solution-growth processes for the synthesis of nanostructure TiO<sub>2</sub>.<sup>12)</sup> In particular, it is well known that various types of TiO<sub>2</sub> nanostructures can be synthesized through strong acid treatment under hydrothermal or non-hydrothermal conditions.<sup>13)</sup>

Herein, we synthesized rutile TiO<sub>2</sub> branched nanostructures (TiO<sub>2</sub>-BNs) for LIBs via hydrothermal process without any surfactant and template. The structural characterization of the TiO<sub>2</sub>-BNs was performed using high-resolution transmission electron microscopy (HR-TEM), fast Fourier transform (FFT), X-ray diffraction (XRD) analysis, and nitrogen sorption measurement. To analyze the performance for LIBs using the TiO<sub>2</sub>-BNs as an anode, charge-discharge and rate cycling curves of the electrodes were measured using a lithium coin cell at room temperature.

## 2. Experimental

For the preparation of seeds of TiO<sub>2</sub>-BNs, 8 mL of titanium(IV) isopropoxide (TTIP (97%), Aldrich) was dropped in 40 mL of 10 M hydrochloric acid (HCl (35%), Aldrich) with constant stirring at 25°C

\*E-mail: kwpark@ssu.ac.kr

for 1 h and then kept at 120°C for 24 h. After the hydrothermal process, the resulting precipitates were cooled to room temperature, washed several times with ethanol and distilled water, and then precipitated using centrifuge at 10,000 rpm. The white TiO<sub>2</sub> seeds were obtained after drying at 50°C oven. The TiO<sub>2</sub>-BN was synthesized by means of a seeding method with TiO<sub>2</sub> seeds. The seed-solution (12 wt%) was injected in 30 mL of 0.5 M HCl with constant stirring at 25°C and then kept constant for 15 min. After that, the 2 mL of TTIP as precursor was dropped in mixture solution and kept constant for 1 h and kept at 90°C for 4 h. The resulting precipitates were cooled to 25°C, washed several times with ethanol and distilled water, and precipitated using centrifuge at 8,000 rpm, and then dried at 50°C drying oven.

The morphology and size distribution of the samples were characterized by FE-TEM (a Tecnai G2 F30 system) operating at 300 kV. TEM samples were prepared by placing drops of powder suspension dispersed in ethanol on a carbon-coated copper grid. XRD analysis was carried out using Rigaku X-ray diffractometer with Cu K<sub>α</sub> ( $\lambda = 0.15418$  nm) source with a Ni filter. The source was operated at 40 kV and 100 mA. The  $2\theta$  angular scan from 20° to 60° was explored at a scan rate of 5° min<sup>-1</sup>. The resolution in the scans was kept at 0.02°. Nitrogen adsorption and desorption isotherms were measured at 77 K using a Micromeritics ASAP 2020. Before the adsorption measurements, all samples were outgassed at 473 K for 360 min in the port of the adsorption analyzer. The starting relative pressure was 0.995 P/P<sup>0</sup> and ending relative pressure was 0.01 P/P<sup>0</sup>.

The electrodes were prepared by mixing 70 wt% TiO<sub>2</sub>-BN as an active material, 20 wt% acetylene black as a conducting agent, and 10 wt% polyvinylidene fluoride (PVDF) as a binder. In order to obtain the slurry, several drops of N-methylpyrrolidone were added into the mixture of TiO<sub>2</sub>-BN with acetylene black and PVDF. The prepared slurry was homogenized by stirring and then coated uniformly on ~11  $\mu\text{m}$  thick copper foil substrates. The electrode dried in an oven at 80°C for 12 h and then cooled down to room temperature. The cells were assembled in a high purity argon filled

glove box using the TiO<sub>2</sub>-BN as the working electrode and lithium foil as the counter and reference electrodes and a separator that was saturated with the electrolyte solution that consisted of 1.1 M LiPF<sub>6</sub> dissolved in a mixture of ethylene carbonate (EC) and dimethyl carbonate (DMC) with a volume ratio of EC/DMC = 1:1.

The lithium intercalation properties of the assembled cells were recorded with charge/discharge curves between 3.0 and 1.0 V. The charge/discharge tests were galvanostatically cycled between 3.0 and 1.0 V for 100 cycles at a current rate of 1 C. After charge/discharge tests for 5 cycles at a current rate of 0.5 C, rate cycle performance tests were also carried out at various current rates from 0.5 to 20 C in order to confirm the rate capability. All of the lithium intercalation measurements were completed at room temperature.

### 3. Results and Discussion

As shown in Fig. 1(a) and (b), the TiO<sub>2</sub>-BNs obtained by a seeding method seem to be a three-dimensional structure with branches grown along one-dimensional backbones. The diameter and length of the TiO<sub>2</sub>-BNs are ~20 and ~110 nm,

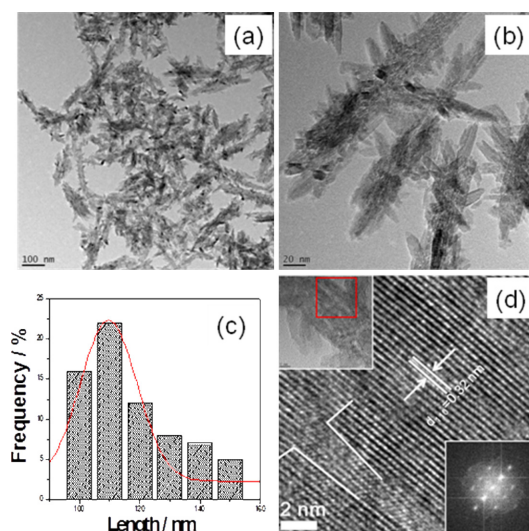


Fig. 1. (a), (b) TEM images of TiO<sub>2</sub>-BNs; (c) Size-distribution histogram of TiO<sub>2</sub>-BNs; (d) HR-TEM image of TiO<sub>2</sub>-BNs (The insets indicate a TEM image of TiO<sub>2</sub>-BNs and the corresponding FFT pattern.).

respectively (Fig. 1(c)). As shown in Fig. 1(d) of high-resolution TEM image, the  $\text{TiO}_2\text{-BN}$  was exposed to (110) plane corresponding to  $d$ -spacing of 0.32 nm. The FFT pattern of the inset in the Fig. 1(d) indicates the (101) and (110) plane of rutile phases. Fig. 2 shows the XRD pattern of the  $\text{TiO}_2\text{-BNs}$  representing rutile phase with tetragonal crystal structure ( $a = b = 0.452$  nm,  $c = 0.294$  nm, space group  $P4_2/mmm$ ). According to the reference (JCPDS No. 88-1175) of the  $\text{TiO}_2$  rutile phase, the

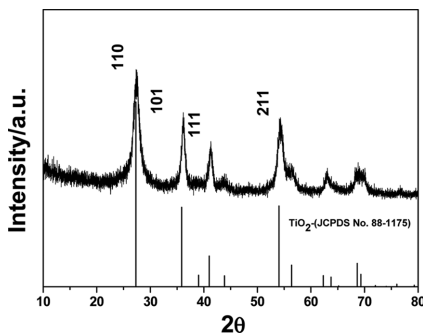


Fig. 2. Wide-angle XRD pattern of  $\text{TiO}_2\text{-BNs}$ .

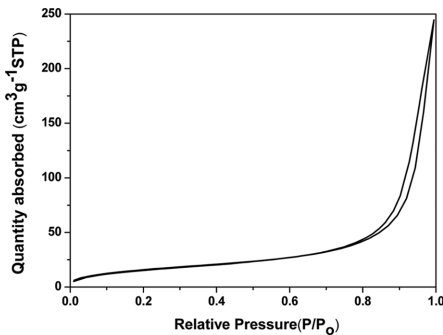


Fig. 3. Nitrogen adsorption/desorption isotherm curve of  $\text{TiO}_2\text{-BNs}$ .

$\text{TiO}_2\text{-BNs}$  show the similar intensity ratio of the principal XRD peaks to that of the reference. As shown in Fig. 3. The BET specific surface area of the  $\text{TiO}_2\text{-BNs}$  is  $\sim 60.3$   $\text{m}^2\text{g}^{-1}$  and is much larger than that of the typical rutile  $\text{TiO}_2$  nanoparticles.<sup>9)</sup>

Fig. 4(a) shows 1<sup>st</sup> and 2<sup>nd</sup> discharge-charge curves of the  $\text{TiO}_2\text{-BNs}$  at a current density of 1 C. At the cycling rate of 1 C, the first charge capacity of the  $\text{TiO}_2\text{-BNs}$  is  $300$   $\text{mAh}\cdot\text{g}^{-1}$  and much larger than that of the typical rutile  $\text{TiO}_2$  electrode.<sup>9)</sup> Furthermore, the  $\text{TiO}_2\text{-BNs}$  as a rutile  $\text{TiO}_2$  electrode exhibit an irreversibility between 1<sup>st</sup> and 2<sup>nd</sup> cycle and two plateaus due to phase transition from rutile to spinel and then rock salt.<sup>14,15)</sup> The cycling performance and coulombic efficiency of the  $\text{TiO}_2\text{-BNs}$  at a current rate of 1 C for 100 cycles are indicated in Fig. 4(b). The  $\text{TiO}_2\text{-BNs}$  exhibit the reversible capacity of  $\sim 190$   $\text{mAh}\cdot\text{g}^{-1}$  and high coulombic efficiency of  $\sim 92.5\%$  up to 100 cycles. To investigate rate cycling performance of the  $\text{TiO}_2\text{-BN}$  electrode, the discharge-charge rates were increased stepwise from 0.5 to 20 C as indicated in Fig. 4(c), the specific charge capacities of  $\text{TiO}_2\text{-BNs}$  are  $215$   $\text{mAh}\cdot\text{g}^{-1}$  at 0.5 C;  $119$   $\text{mAh}\cdot\text{g}^{-1}$  at 5 C;  $43$   $\text{mAh}\cdot\text{g}^{-1}$  at 20 C. This represents that even at high current rates from 5 to 20 C,  $\text{TiO}_2\text{-BNs}$  can display an excellent rate cycling performance. The remarkably large capacity of  $216$   $\text{mAh}\cdot\text{g}^{-1}$  can be obtained when the current rate is returned to 0.5 C after 60 cycles at different current rates. The improved lithium-ion intercalation properties of  $\text{TiO}_2\text{-BNs}$  may be attributed to large specific surface area, short transport distance of nanostructure, and freedom for volume change accompanied by lithium-ion intercalation.<sup>16)</sup>

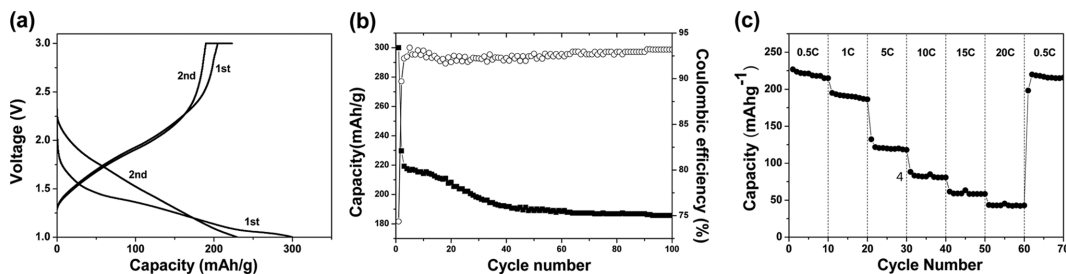


Fig. 4. (a) 1<sup>st</sup> and 2<sup>nd</sup> discharge-charge curves of the  $\text{TiO}_2\text{-BNs}$  at a current density of 1 C; (b) The cycling performance and coulombic efficiency of the  $\text{TiO}_2\text{-BNs}$  at a current rate of 1 C for 100 cycles; (c) Rate capability of the  $\text{TiO}_2\text{-BNs}$  from 0.5 C to 20 C.

#### 4. Conclusions

In summary, using seeding method in hydrothermal process without any surfactant and template, we have prepared three-dimensional TiO<sub>2</sub>-BN anode materials. The TiO<sub>2</sub>-BNs showed large capacity, high coulombic efficiency, and excellent high rate cycling performance in lithium intercalation properties, and the facilitating lithium ion motion in the nanostructure electrode.

#### Acknowledgments

This work was supported by the Soongsil University Research Fund of 2009.

#### References

1. J.-M. Tarascon and M. Armand, 'Issues and challenges facing rechargeable lithium batteries' *Nature*, **414**, 359 (2001).
2. M. S. Whittingham, 'Lithium batteries and cathode materials' *Chem. Rev.*, **104**, 4271 (2004).
3. Y.-K. Zhou, L. Cao, F.-B. Zhang, B.-L. He, and H.-L. Li, 'Lithium insertion into TiO<sub>2</sub> nanotube prepared by the hydrothermal process' *J. Electrochem. Soc.*, **150**, A1246 (2003).
4. M. Grätzel, 'Photoelectrochemical cells' *Nature*, **414**, 338 (2001).
5. J. Xu, C. Jia, B. Cao, and W. F. Zhang, 'Electrochemical properties of anatase TiO<sub>2</sub> nanotubes as an anode material for lithium-ion batteries' *Electrochim. Acta.*, **52**, 8044 (2007).
6. A. L. Linsebigler, G. Lu, and J. T. Yates, 'Photocatalysis on TiO<sub>2</sub> surfaces: principles, mechanisms, and selected results' *Chem. Rev.*, **95**, 735 (1995).
7. M. A. Fox and M. T. Dulay, 'Heterogeneous photocatalysis' *Chem. Rev.*, **93**, 341 (1993).
8. M. S. Chen and D. W. Goodman, 'The structure of catalytically active gold on titania' *Science*, **306**, 252 (2004).
9. B. Han, S.-J. Kim, B.-M. Hwang, S.-B. Kim, and K.-W. Park, 'Single-crystalline rutile TiO<sub>2</sub> nanowires for improved lithium ion intercalation Properties' *J. Power Sources*, **222**, 225 (2013).
10. P. Segovia, D. Purdie, M. Hengsberger, and Y. Baer, 'Observation of spin and charge collective modes in one-dimensional metallic chains' *Nature*, **402**, 504 (1999).
11. A. S. Nair, Y. Shengyuan, Z. Peining, and S. Ramakrishna, 'Rice grain-shaped TiO<sub>2</sub> mesostructures by electrospinning for dye-sensitized solar cells' *Chem. Commun.*, **46**, 7421 (2010).
12. D. J. Hombaker, S.-J. Kahng, S. Misra, B. W. Smith, A. T. Johnson, E. J. Mele, D. E. Luzzi, and A. Yazdani, 'Mapping the one-dimensional electronic states of nanotube peapod structures' *Science*, **295**, 828 (2002).
13. A. Kumar, A. R. Madaria, and C. Zhou, 'Growth of aligned single-crystalline rutile TiO<sub>2</sub> nanowires on arbitrary substrates and their application in dye-sensitized solar cells' *J. Phys. Chem. C*, **114**, 7787 (2010).
14. M. Vijayakumar, S. Kerisit, C. Wang, Z. Nie, K. M. Rosso, Z. Yang, G. Graff, J. Liu, and J. Hu, 'Effect of chemical lithium insertion into rutile TiO<sub>2</sub> nanorods' *J. Phys. Chem. C*, **113**, 14567 (2009).
15. W. J. H. Borghols, M. Wagemaker, U. Lafont, E. M. Kelder, and F. M. Mulder, 'Impact of nanosizing on lithiated rutile TiO<sub>2</sub>' *Chem. Mater.*, **20**, 2949 (2008).
16. C. H. Sun, X. H. Yang, J. S. Chen, Z. Li, X. W. Lou, C. Li, S. C. Smith, G. Q. Lu, and H. G. Yang, 'Higher charge/discharge rates of lithium-ions across engineered TiO<sub>2</sub> surfaces leads to enhanced battery performance' *Chem. Commun.*, **46**, 6129 (2010).